Marine Chemistry 241 (2022) 104106

Contents lists available at ScienceDirect

Marine Chemistry

journal homepage: www.elsevier.com/locate/marchem

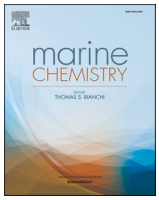

The effect of aerosol size on Fe solubility and deposition flux: A case study in the East China Sea

Chih-Chiang Hsieh [a,b], Hung-Yu Chen [c], Tung-Yuan Ho [a,b,*]

[a] Research Center for Environmental Changes, Academia Sinica, Taipei, Taiwan
[b] Institute of Oceanography, National Taiwan University, Taipei, Taiwan
[c] Department of Marine Environmental Informatics, National Taiwan Ocean University, Keelung, Taiwan

ARTICLE INFO

Keywords:
Aerosol
Dissolved Fe
Labile Fe
Size-fractionated aerosol
Solubility
Deposition flux
The East China Sea
GEOTRACES

ABSTRACT

Aerosol sizes are highly associated with the solubilities and the deposition fluxes of aerosol Fe in the surface ocean since the sizes may reflect the sources and decide the deposition velocities. However, systematic studies for the association of the solubilities and fluxes have been limited. In this study, five size-fractions of dry aerosols were collected monthly for a year at two islets in the East China Sea, where large amounts of both fine anthropogenic and coarse lithogenic aerosols deposit. Both pure water and buffer leached methodologies were applied to determine the two operationally defined dissolvable Fe fractions, instantly dissolved Fe (DFe) and supposedly Fe-ligand complexed labile Fe (LFe), respectively. We found that the solubilities of DFe varied up to 4 orders of magnitude with the size spectrum and exhibited a highly linear correlation with non-sea-salt sulfur, indicating that the solubilities of DFe were closely associated with the acidity. Finer aerosols (PM 3) accounted for 90% of total DFe but coarser aerosols (>PM 3) contributed 66% of the difference between LFe and DFe (LFe-DFe). The increasing trend of the difference with increasing sizes indicates that the residence time of coarse aerosol particles and their interaction with Fe-ligands are critical factors deciding the total fluxes of LFe in the ocean. Considering the deposition velocities of each size of aerosols, the averaged fluxes of aerosol Fe of the fine and coarse aerosols were 1.8 and 5.9 nmol m^{-2} d^{-1} for DFe; and 2.8 and 62 nmol m^{-2} d^{-1} for LFe in the East China Sea, respectively. Attributed to the relatively low deposition velocities of fine aerosols, we found that either single or two averaged deposition velocities (fine/coarse) that were used in most of the previous studies would significantly overestimate dissolvable Fe fluxes in regions where the contribution of fine anthropogenic aerosols is dominant, such as the open ocean. In conclusion, this study demonstrates that aerosol sizes are essential and powerful parameters to accurately estimate the solubility and the fluxes of aerosol dissolvable Fe.

1. Introduction

Since iron (Fe) is a major limiting micronutrient for phytoplankton growth in the large area of the global ocean, Fe supply in the euphotic zone may affect the oceanic biological pump and global carbon cycling (Martin, 1990; Martin and Fitzwater, 1988). Aerosol deposition is a major process supplying external Fe to the euphotic zone of the surface ocean so that the quantification of aeolian bioavailable Fe supply in the surface water is crucial to study biological pump and material cycling in the ocean (Jickells et al., 2005; Tagliabue et al., 2017). Aerosol dissolvable Fe is generally considered to be bioavailable to marine phytoplankton (Raiswell and Canfield, 2012). However, the quantification of aerosol dissolvable Fe in the euphotic zone of the ocean is a highly challenging task operationally, attributed to the extremely complicated atmospheric and aquatic physicochemical processes and reactions involved in aerosol transport and the post-deposited phase transformation of aerosol dissolvable Fe in the surface water (Meskhidze et al., 2019).

The lack of a standard methodology for assessing aerosol dissolvable iron is a major challenge (Meskhidze et al., 2019). Aerosol dissolvable or bioavailable Fe can be separated into two fractions, dissolved Fe (DFe) and labile Fe (LFe). Operationally, DFe is defined as instantly dissolved aerosol Fe in pure water or seawater that passes through 0.2 μm filter (Buck et al., 2006); LFe stands for buffer or acid leached Fe to present for Fe release from aerosols in rainwater (Baker et al., 2006; Sarthou et al., 2003) or Fe-ligand complexed fraction that may be bioaccessible

* Corresponding author at: 128, Sec. 2, Academia Rd., Nankang, Taipei 115, Taiwan.
E-mail address: tyho@gate.sinica.edu.tw (T.-Y. Ho).

https://doi.org/10.1016/j.marchem.2022.104106
Received 20 August 2021; Received in revised form 21 February 2022; Accepted 17 March 2022
Available online 26 March 2022

(Perron et al., 2020b). DFe and LFe can thus be referred to the lower and upper limits of bioavailable aerosol Fe post-deposited in the surface ocean, respectively (Perron et al., 2020b), and the comparison of DFe and LFe fractions among different studies would require standardized leaching protocols. However, previous studies on the measurement of aerosol Fe solubility have used various leaching methods with different extraction solutions, pH, or leaching time et al. Large discrepancies of the solubility of DFe and LFe are observed. Baker et al. (2016) recommended using a common reference aerosol material to decide the solubilities (Arizona Test Dust or ATD, Powder Technology Inc.). Perron et al. (2020b) proposed a 3-step leaching protocol combining commonly used approaches to obtain DFe and LFe in aerosols, in which DFe is obtained by super pure water instant leach and LFe is by soaking aerosol samples in 1.1 M ammonia acetate buffer solution at pH 4.7 for 1 h to mimic Fe-ligand complexation. For future studies, it is necessary to measure the solubilities of DFe and LFe in aerosol Fe studies by using comparable approaches.

Sampling aerosols across a range of sizes is an additional challenge. Although aerosol size is a critical factor reflecting the sources and influencing the deposition velocities, limited studies reported size-fractionated information in marine aerosol field observations (Baker et al., 2020; Buck et al., 2010; Gao et al., 2020; Kurisu et al., 2016; Sakata et al., 2018; Yang et al., 2020), mainly due to the limited sampling time to obtain sufficient masses in cruises. On the other hand, relatively long aerosol sampling time may encounter highly varying meteorological conditions, which may introduce uncertainty for flux estimates. The estimates of aerosol Fe deposition fluxes of previous studies have been mostly based on bulk aerosol Fe concentrations and fixed average deposition velocity (Buck et al., 2013; Hsu et al., 2010; Perron et al., 2020a). The deposition velocities used to estimate aerosol Fe fluxes are generally oversimplified and may introduce large uncertainties (Duce et al., 1991). As pointed out by Foret et al. (2006), increasing the number of size bins would significantly increase the accuracy of the estimate of the fluxes. Moreover, aerosol sizes may reflect their sources. For example, size-fractionated aerosols exhibited significantly different Fe solubilities and composition (Kurisu et al., 2016). As far as we know, the effects of aerosol sizes on the solubilities and the deposition fluxes of aerosol Fe have not been systematically studied in the surface ocean.

Right next to mainland China, the East China Sea receives a large amount of fine anthropogenic and coarse lithogenic aerosols from the continent, serving as an excellent sampling region for the size study. Selecting two islets in the marginal sea, we have systematically investigated DFe and LFe solubilities among five different size-fractionated dry aerosols collected at two islets in the oceanic region for one year by following the standard protocols proposed (Perron et al., 2020b). We have also evaluated the discrepancy of the deposition fluxes caused by using different deposition velocities of aerosols. The findings of this study shall provide insights for the impacts of aerosol sizes on the solubility and the fluxes and how to obtain a more accurate estimate of the deposition fluxes of aerosol dissolvable Fe regionally and globally.

2. Method

2.1. Sampling sites and methods

Size-fractionated aerosol samples were collected on polytetrafluoroethylene (PTFE) filters (TE-230-PTFE, Tisch Environmental Inc., US) by using a high volume air sampler (TISCH Environmental Inc., US, MODEL-TE-5170) with a cascade impactor (TISCH Environmental Inc., US, Series 235) on the roofs of buildings in Matsu Island (26.17°N; 119.92°E; with height about 6 m above the ground) and Pengjia Islet (25.63°N; 122.08°E; with height about 6 m above the ground) from September 2019 to August 2020 (Fig. 1). The flow rates of the samplers were calibrated once per month, and the averaged flow rates were 1.0 ± 0.1 m^{-3} min^{-1}. The sampling sites of Matsu Island and Pengjia Islet are

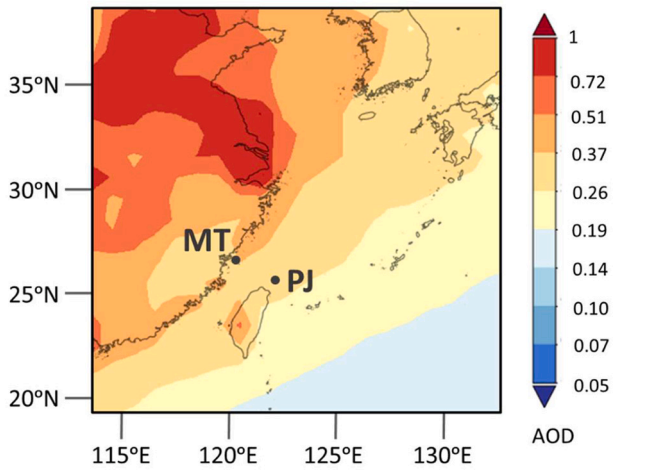

Fig. 1. The location of the sampling stations, Matsu island (MT) and Penjia islet (PJ), and the decadal averaged aerosol optical depths from 2010 to 2020. The aerosol optical depth data were obtained by NASA Giovanni software (https://giovanni.gsfc.nasa.gov/giovanni/).

abbreviated as MT and PJ in the text hereafter, respectively. MT station is close to mainland China, only about 19 km from Fujian province, with area to be 30 km^2 and population to be 12,700. On the other hand, mainly composed of igneous minerals, PJ station is a small islet with area to be 1.1 km^2 and about 66 km from the northernmost of Taiwan (Fig. 1). Except governmental staff who carry out routine meteorological monitoring, there are no anthropogenic activities on PJ, which would thus be ideal to serve as a representative aerosol sampling site for the East China Sea. Monthly aerosol samples were obtained by collecting dry aerosols for 7–8 days continuously in each month, but not included the months of September, December, January, and July for MT and October and November for PJ due to temporary breakdown and regular maintenance of the samplers. The cascade impactor separated aerosols into five size fractions, the size cut-offs including stage 1, 7.3 μm; stage 2, 3.1 μm; stage 3, 1.6 μm; stage 4, 1.0 μm; and stage 5, 0.57 μm (Table 1). To simplify some of the discussion for size fractions, we have separated the five fractions into coarse and fine modes by using 3 μm as the cut-off. Fine and coarse aerosols mentioned in this study refer to PM $\leq$ 3 (the sum of sizes 0.57, 1.0, and 1.6 μm) and PM > 3 (the sum of sizes 3.1 and 7.3 μm), respectively (Table 1). Sampling filters were freeze-dried and weighed at constant humidity before and after sampling. The filters with aerosols were then stored in a -20 °C freezer before further chemical processes. It should be noted that PM $\leq$ 3 may still contain a small amount of lithogenic aerosols and vice versa, although the two size fractions may be representative for anthropogenic and lithogenic aerosols in general. We would like to point out that the impactors did not produce equal distributions of particles across all 10 slots of the substrate. We have used the software ImageJ to quantify the relative proportion by the intensity of the grayscale image in each slot and to calculate the total concentrations of the whole filters.

2.2. Quantification of DFe, LFe, and TFe

All chemicals used in this study were ultra-high purity grade, including nitric acid, hydrochloric acid, hydrofluoric acid, ammonium

Table 1
The information of the size cut-offs and size ranges of size-fractionated aerosols collected in this study.

Impactor stage	5	4	3	2	1
Size range (μm)	0.57–1.0	1.0–1.6	1.6–3.1	3.1–7.3	>7.3
Size cut-off (μm)	0.57	1.0	1.6	3.1	7.3

hydroxide, and acetic acid (J.T. Baker). All of the laboratory procedures were carried out in a positive pressured class 5 cleanroom, either in a HEPA-filtered class 5 laminar flow bench or hood. Powder-free polyvinyl chloride (PVC) gloves were worn while handling samples. We followed the suggested protocols of the GEOTRACES Cookbook to carry out the cleaning procedures for storage vials and sample digestion (Cutter et al., 2017).

For leaching procedures, we have followed the protocols suggested by Perron et al. (2020b) and made some modifications. The fractions of dissolved (DFe), labile (LFe), and total Fe (TFe) concentrations in aerosols were defined by three different digestion and leaching protocols. The samples for the three fractions were obtained from different slots of filters. DFe was leached by 5 mL of ultrapure water (Millipore Elix plus Element purification system) with gentle shaking for 10 s, then filtered through a 13 mm pre-acid washed polypropylene syringe filter with 0.2 μm hydrophilic PTFE membrane (Advantec) into a pre-acid washed 15 mL polypropylene vial (Buck et al., 2006). The LFe leach was processed using another aerosol filter soaked in 8 mL of ammonium acetate (1.4 M, pH 4.7) for 1 h. Then, the samples were centrifuged after removing the filter (Baker et al., 2006; Sarthou et al., 2003). The supernatant was collected by an autopipette for the quantification of target elements. TFe was obtained by digesting aerosol samples using a freshly prepared mixture of 4 M HF, 4 M HCl, and 4 M HNO_3 for 4 h at 120 °C (Ohnemus et al., 2014). The blank concentrations were measured by processing new filters with same digestion procedures as samples. The concentration levels of almost all of the digested samples were at least two orders of magnitude higher than the blank value for TFe, DFe, and LFe, which were 0.13, 0.036, and 0.023 pmol m^{-3}, respectively (Table S1 & S2).

The leachates and digests were diluted by super ultrapure water to obtain the final concentration of 0.5 M HNO_3 and with 1 ppb of indium as an internal standard. All of the samples were analyzed by a sector field high resolution ICP-MS (Element XR, Thermo Fisher Scientific). The detailed information of the analytical method, blank, precision, accuracy was reported in our previous studies (Ho et al., 2010; Wang et al., 2014). In brief, the isotopes of ^{115}In, ^{207}Pb and ^{208}Pb were determined at low resolution (M/ΔM ~ 300), ^{27}Al, ^{32}S, ^{47}Ti, ^{49}Ti, ^{51}V, ^{31}P, ^{54}Fe, ^{56}Fe, ^{60}Ni, ^{61}Ni, and ^{115}In were analyzed at medium resolution (M/ΔM ~ 4000), and ^{23}Na, and ^{115}In were determined at high resolution (M/ΔM ~ 10,000). Na and S were only determined in the dissolved fraction, and all other elements were determined in all fractions. We also used Arizona Test Dust (ATD, <3 μm, Powder Technologies Inc.) and NIES CRM No. 28 Urban Aerosols collected in Beijing (BJ, National Institute for Environmental Studies) as reference material for accuracy validation. The ratios of our measured value to the previously reported value for Arizona test dust were 92% (Al), 100% (Ti), 102% (V), and 97% (Fe) (Shelley et al., 2015); The ratios to the certified values for urban aerosol reference material, NIES CRM No. 28, were 92% (Al), 93% (Ti), 101% (V), 97% (Fe), 114% (Ni), and 99% (Pb) (Table S3). The concentrations and solubilities of DFe and LFe in these two reference materials were also reported in Table 2 for future comparison from other laboratories. The solubilities of DFe or LFe were calculated as the leached concentration ratios of either DFe or LFe to TFe concentrations.

Table 2
The concentrations and solubilities of DFe and LFe in the two reference materials, Arizona Test Dust (ATD) and NIES CRM No. 28 Urban Aerosols (BJ).

Sample	n	Concentration		Solubility (%)	
		DFe	LFe	DFe	LFe
Blank (ng)	5	1.7 ± 1.1	2.1 ± 1.5	–	–
ATD (mg g^{-1}) (↓)	3	3.8 ± 0.7	347 ± 13	0.013 ± 0.002	1.2 ± 0.1
BJ (mg g^{-1})	3	351 ± 29	1360 ± 24	1.2 ± 0.1	4.7 ± 0.1

2.3. The calculation of fluxes, enrichment factors, and non-sea-salt sulfur

We calculated the fluxes by multiplying size-fractionated aerosol Fe concentrations measured (TFe, DFe, or LFe) with their individual deposition velocities:

$$F_{dry} = \sum_{i=1}^{5} C_{Fe\_i} * V_{d\_i}$$

The term, C_{Fe_i}, refers to the concentrations of aerosol Fe measured in each size fraction, and V_{d_i} represents the dry deposition velocity of each size range. The velocity is a function of aerosol sizes and atmospheric conditions, which are mainly decided by wind speed, relative humidity, and sea surface temperature. Since the relative humidity were extremely high at the sampling sites (Table S4), we have calculated the velocities of size-fractionated aerosols by assuming humidity equilibrium condition. Meteorological data of the sampling sites were obtained from the reports of the Weather Bureau of Taiwan (https://e-service.cwb.gov.tw/, Table S4) and the velocities were calculated by using the model proposed previously (Emerson et al., 2020; Quinn and Ondov, 1998; Slinn and Slinn, 1980). The velocities estimated are comparable to the value estimated by a recent study (Emerson et al., 2020).

The enrichment factors (EF) of some specific metals, such as Pb and V, are useful indicators to distinguish anthropogenic aerosols from natural lithogenic dusts (Jickells et al., 2016; Shelley et al., 2017; Sholkovitz et al., 2009). Titanium (Ti) has been shown to be a more reliable proxy to present the mass of upper or bulk continental crust than Al (Lam et al., 2015). The EF presented in this study would be calculated by the total mass ratios of the metals to Ti measured in aerosols divided by the ratio of the upper continental crust (UCC):

$$EF_{Pb} = (Metals/Ti)_{aerosol} / (Metals/Ti)_{UCC}$$

The term, $(Metals/Ti)_{UCC}$, is the reference value of the upper continental crust cited from Hu and Gao (2008).

Acidic conditions on aerosol surfaces in the atmosphere solubilize mineral Fe in aerosol particles (Meskhidze et al., 2003; Zhu et al., 1992). Aerosol acidity is mainly decided by the concentrations of SO_2, NO_x, and NH_3 and its aeolian transport processes (Baker et al., 2021). Buck et al. (2006) found the acidity of the aerosol samples has a significant correlation with the concentrations of dissolvable Fe in the North Western Pacific Ocean (NWPO) and non-sea-salt (nss-) sulfate is the major acidity contributor. Indeed, nss-sulfate accounts for a major fraction of aerosol acidity in our studied region. Normalized to nitrate acidity, the molar ratios of the acidities of nss-sulfate and ammonium were 2.5 and 2.3 in the East China Sea, 2.8 and 2.1 at Cape Fuguei station, and 5.5 and 3.9 at Penghu (Chou et al., 2008; Hsu et al., 2010), respectively. Although the acidity from nss-sulfate cannot represent total aerosol acidity, it is a good proxy for the variations of total aerosol acidity in our studied region. In this study, we have measured Na and total S and assume that nss-S is mainly from nss-sulfate and the concentrations were calculated by subtracting the sulfate contribution from sea salt to the aerosols:

$$[\text{nss-}S] = [S] - [\text{Na}] \times (S/\text{Na})_{seawater}$$

The terms, [S] and [Na], are the dissolved concentrations of sulfur and sodium measured by ICPMS, and $(S/Na)_{seawater}$ stands for the molar ratio of S to Na in seawater, which is 0.060.

3. Result and discussion

3.1. The distribution patterns of aerosol Fe concentrations

The prevailing seasons of northeastern (NE) and southwestern(SW) monsoons in our studied region are October to April and May to September, respectively. We found that the contribution of anthropogenic type elements (e.g., Pb or V) was generally higher in the NE monsoon period than in the SW period (Fig. S1 & S2). The ratios of EF_{Pb} and EF_V between the NE and SW seasons ranged from 2.2 to 4.8 and from

1.3 to 2.9-fold at PJ, respectively, generally showing decreasing ratios with increasing sizes. The ratios for EF_{Fe} were 1.4, 1.0, 1.1, 1.2, and 1.1-fold for the aerosols from the smallest to the largest. As the seasonal variations of Fe were insignificant for most of the size fractions, the seasonality was not discussed in this study.

Generally, the masses of fine aerosols were less than coarse aerosols, with average values to be 15 and 19 μg m^{-3} at MT and 11 and 25 μg m^{-3} at PJ (Table S6), respectively. As expected, the concentrations of total aerosol Fe generally increased with increasing particle sizes for the two sampling stations for almost all of the sampling time. On average, the concentrations were 531, 938, 1743, 3849, and 3097 pmol m^{-3} with increasing sizes at MT and 194, 368, 721, 1780, and 2368 pmol m^{-3} at PJ (Fig. 2, Table S7). The average TFe at MT was about twice that of PJ. Based on the 5-day air mass back trajectories (Fig. S1), the relatively high TFe observed for MT was probably attributed to the relative high percentage of the aerosol transport pathways close to eastern mainland China. However, the concentrations of DFe exhibit opposite patterns with aerosol sizes. On average, the concentrations of DFe were 121, 46, 9.0, 9.5, and 2.6 pmol m^{-3} at MT and 74, 27, 12, 9.3, and 3.6 pmol m^{-3} at PJ (Fig. 2, Table S7). The differences between TFe and DFe increased with increasing particle sizes for both stations and was up to 3 orders of magnitude for size 7.3 μm, showing that the coarse fraction accounted for most of non-instantly dissolvable Fe. The average concentrations of LFe were 116, 60, 30, 46, and 48 pmol m^{-3}, and 67, 36, 28, 38, and 42 pmol m^{-3} for MT and PJ, respectively (Fig. 2, Table S7). The concentrations of LFe were similar to DFe for size 0.57 and 1.0 μm but were significantly influenced by TFe for size 1.6, 3.1, and 7.3 μm, indicating that dissolvable Fe in the two fine size fractions was mainly from DFe and dissolvable Fe in the coarse fraction was mainly from LFe.

3.2. The solubility of DFe and the sources

The solubilities of DFe decreased exponentially with increasing particle sizes for both stations in all months, ranging for almost 4 orders of magnitude (Fig. 2, Table S8). The solubilities ranged from 0.011 to 44% and from 0.012 to 74% for MT and PJ, respectively. On average, the solubilities were 25, 7.6, 0.87, 0.41, and 0.19 with increasing sizes at MT and 50, 9.3, 2.2, 0.77, and 0.19 at PJ (Fig. 2, Table S8).

Although both anthropogenic and lithogenic aerosols may have widely spanned size ranges, for most of the oceanic regions, anthropogenic aerosols account for a dominant fraction in fine aerosols (Matsui et al., 2018). Aerosol sizes may thus reflect their sources (Mead et al., 2013) and aerosol Fe solubilities. For example, Schroth et al. (2009) reported that Fe solubility was 0.04% in African dust but was up to 81% in oil fly ash. The enrichment factor of Pb has been used to evaluate the contribution of anthropogenic and lithogenic aerosols in many previous aerosol studies (Jickells et al., 2016; Shelley et al., 2017). In this study, we found that the overall DFe solubility was linearly correlated with

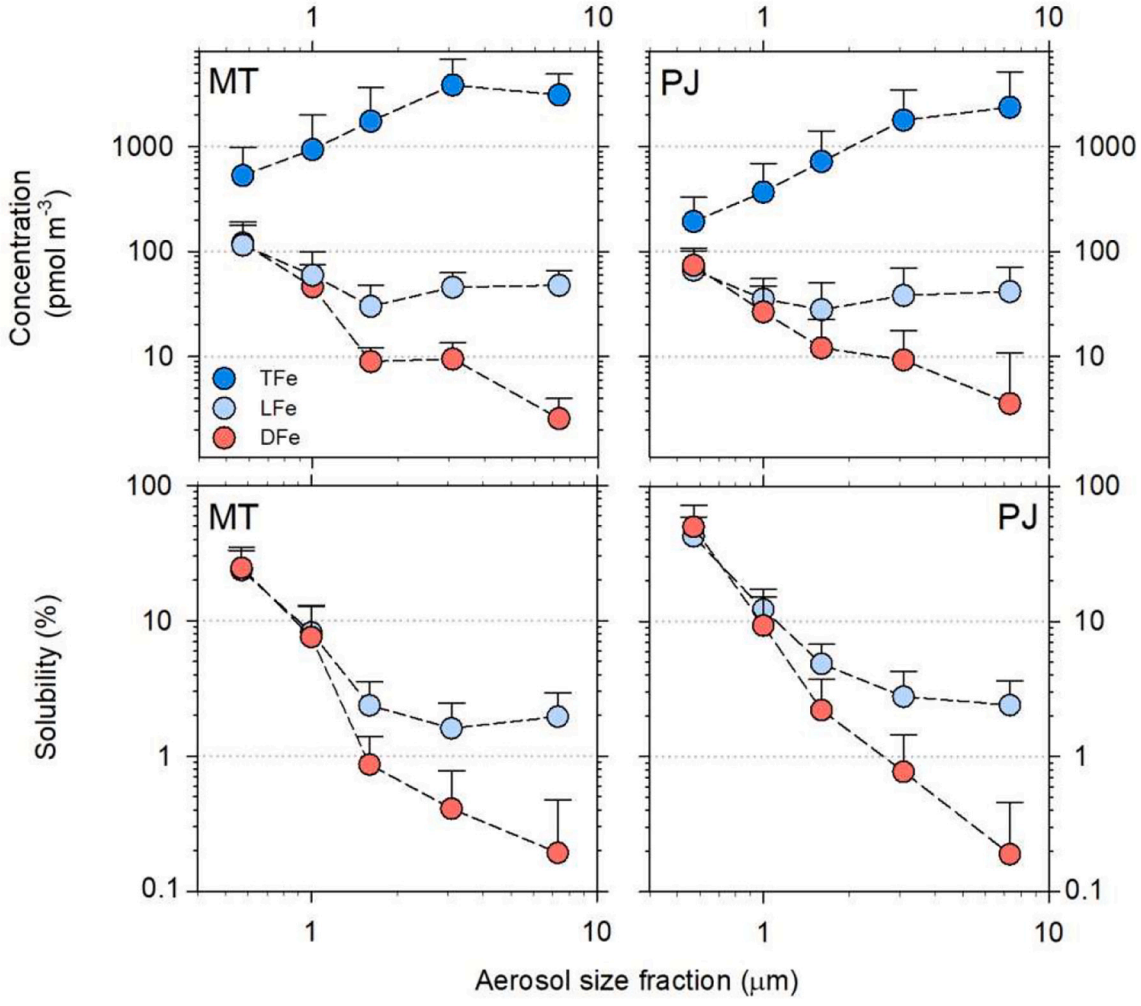

Fig. 2. The averaged concentrations of DFe, LFe, and TFe and the solubility of DFe and LFe in the size-fractionated aerosols collected among different months at MT (left) and PJ (right). Red, light blue, and dark blue symbols stand for DFe, LFe, and TFe, respectively. The deviation bars stand for one standard deviation of all monthly data during the sampling period (Table S7 and S8). (For interpretation of the references to colour in this figure legend, the reader is referred to the web version of this article.)

EF_{Pb} for both stations in this study (Fig. 3). The solubility increased from 0.011 to 74% with EF_{Pb} ranging from 1.5 to 1067 (Fig. 3, Table S9). We also found that the solubility variations within the same size fraction may be up to 1 to 2 orders of magnitude. The variations are positively associated with EF_{Pb} in most of the fractions. For example, the solubility of size 0.57 μm in MT varied from 0.011 to 0.80 with EF_{Pb} increased for about one order of magnitude. In brief, highly associated with the size spectrum and EF_{Pb}, the wide range of the Fe solubilities appears to be associated with the relative contribution of lithogenic and anthropogenic aerosols, suggesting that the two end member physical mixing of lithogenic and anthropogenic aerosols decides the patterns of DFe solubility (Fig. 3).

We have also found that the distribution of DFe and LFe solubilities with EF_{Pb} exhibits a significant spatial difference between MT and PJ but the distribution patterns with EF_V and TFe normalized non-sea-salt sulfur (nss-S) are comparable (Fig. 4). As V serves as a representative metal in heavy oil, the comparable results indicate that the source of aerosols with highly dissolvable Fe and high nss-S are associated with heavy oil burning. Moreover, the distribution of DFe solubility and TFe normalized nss-S exhibits the highest correlation among EF_{Pb}, EF_V, and the TFe normalized nss-S, spanning over 4 orders of magnitude among the 5 size fractions, in comparison to the 2 and 3 orders of magnitude for EF_V and EF_{Pb}, respectively. The strong correlation suggests that the acidity may promote aerosol Fe solubilities in the size-fractionated aerosols.

3.3. The solubility of LFe and the sources

The distribution patterns of LFe solubility exhibit partial dissimilarities with DFe, with a much higher value for the coarse fraction but a relatively comparable value for the fine fraction (Fig. 2). The solubilities ranged from 0.50 to 39% and from 0.78 to 59% for MT and PJ stations, respectively. On average, the solubilities were 24, 8.2, 2.4, 1.6, and 2.0% at MT and 42, 12, 4.8, 2.8, and 2.4% at PJ from size 0.57 to 7.3 μm, respectively (Table S8).

The overall labile solubilities were also linearly correlated with EF_{Pb} for both stations, generally showing increasing solubilities and EF_{Pb} with decreasing sizes (Fig. 3). Limited studies have focused on investigating the causes for the differences between LFe and DFe. Using the same buffer dissolution treatment, Perron et al. (2020b) reported that LFe solubility was 1.4-fold of DFe solubility in total suspended aerosol particles. Using a weak and a strong Fe binding ligand-solution treatment for 1 day, Clough et al. (2019) observed 1.5 and 1.7-fold of DFe solubility, respectively. The LFe solubilities observed in these two studies using bulk aerosols were comparable to our whole size result, 1.9 ± 1.0 (Table S8). All of these previous studies have used total suspended aerosols to carry out the leaching experiments so that the effects of different leaching treatments on lithogenic and anthropogenic aerosols remain unknown. To the best of our knowledge, the differences between DFe and LFe solubilities have not been systematically investigated among size-fractionated aerosols. Our results show that the coarser the sizes the differences of the solubilities between DFe and LFe are larger. The differences were over one order of magnitude for size 7.3 μm, indicating the organic buffer can leach much more extra Fe in coarse aerosols than fine aerosols (Fig. 5). Comparable to the solubilities observed in the size 7.3 μm fraction of this study, the solubilities of LFe we measured in ATD reference material was 1.2%, which is also about two order of the magnitude higher than the solubility of DFe, which is 0.013% (Table 2). The coarse aerosols (>PM 3) contributed majorities of the difference between LFe and DFe masses, 70% for MT and 73% for PJ

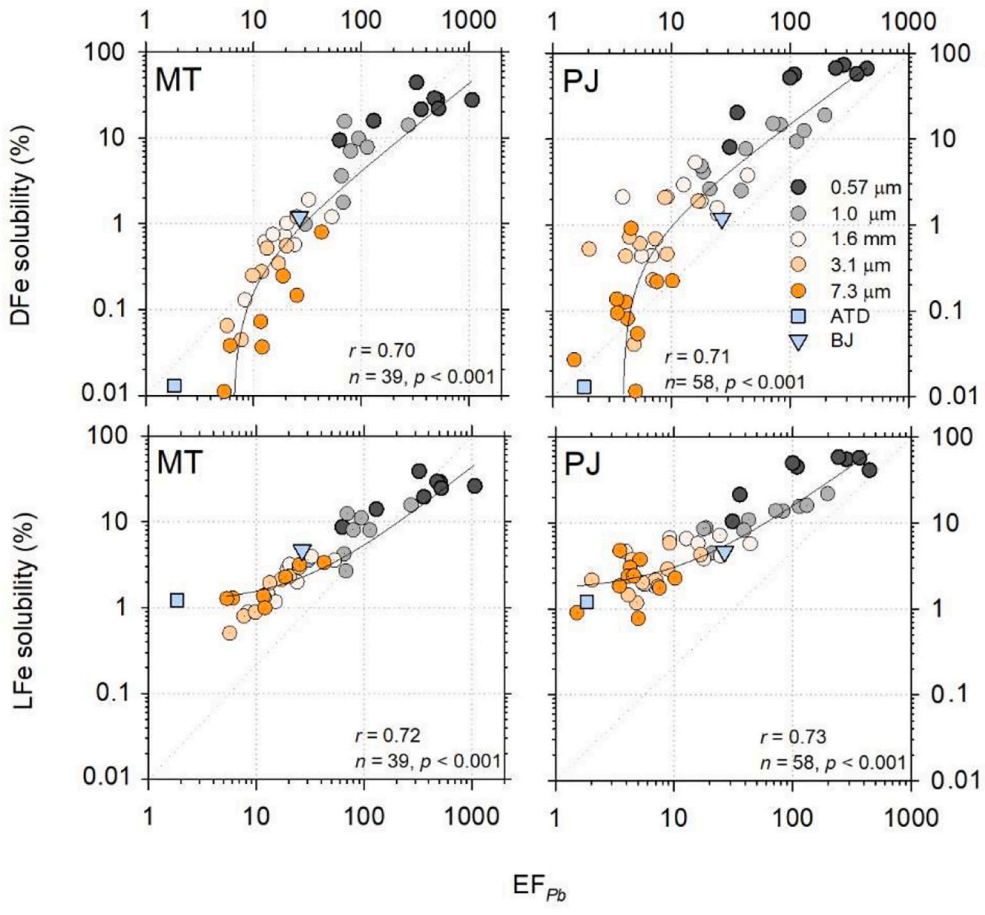

Fig. 3. The comparison of the solubilities of DFe and LFe of the size-fractionated aerosols with the enrichment factor of Pb (EF_{Pb}) at MT (left) and PJ (right). The symbol colors are black for size cut-offs 0.57 μm, gray for 1.0 μm, white for 1.6 μm, light orange for 3.1 μm, and dark orange for 7.3 μm, respectively. ATD and BJ stand for the two reference materials, Arizona Test Dust (light blue square) and NIES CRM No. 28 Urban Aerosols collected in Beijing (light blue triangle), respectively. The solid lines in each plot stand for linear regression lines of the data. (For interpretation of the references to colour in this figure legend, the reader is referred to the web version of this article.)

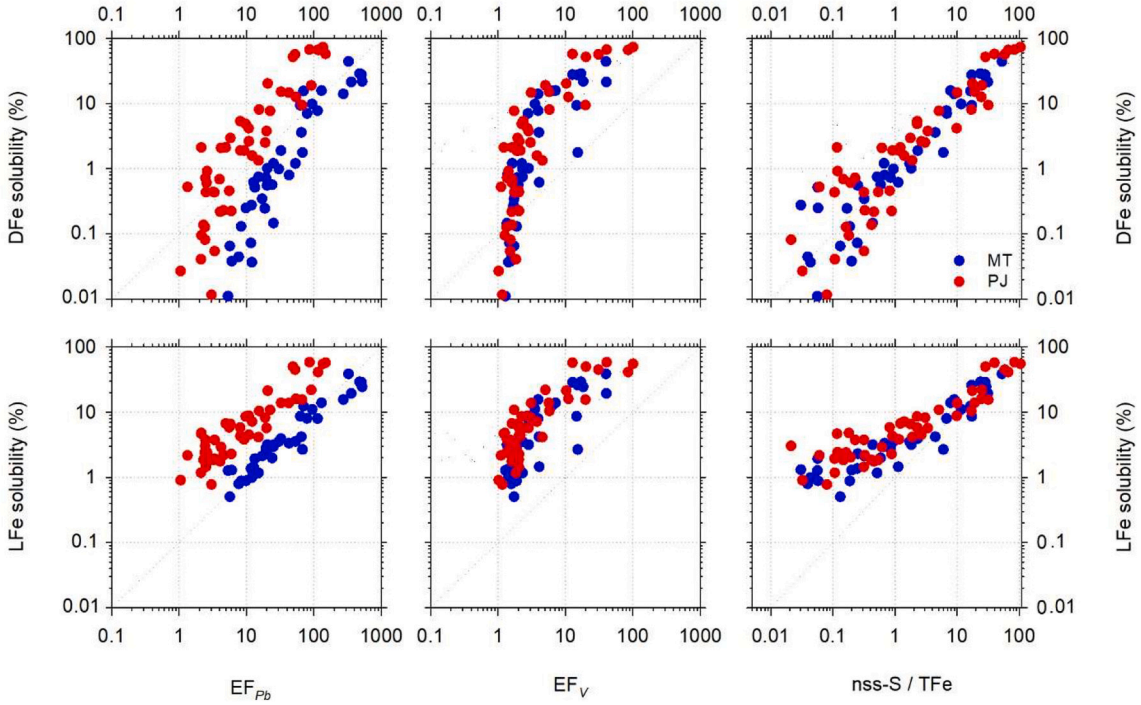

Fig. 4. The comparison of DFe and LFe solubilities with EF_{Pb}, EF_V, and total Fe normalized nss-S among the two sampling sites. The blue circle refers to MT; the red circle refers to PJ. The term, nss-S/TFe, stand for TFe normalized nss-S. (For interpretation of the references to colour in this figure legend, the reader is referred to the web version of this article.)

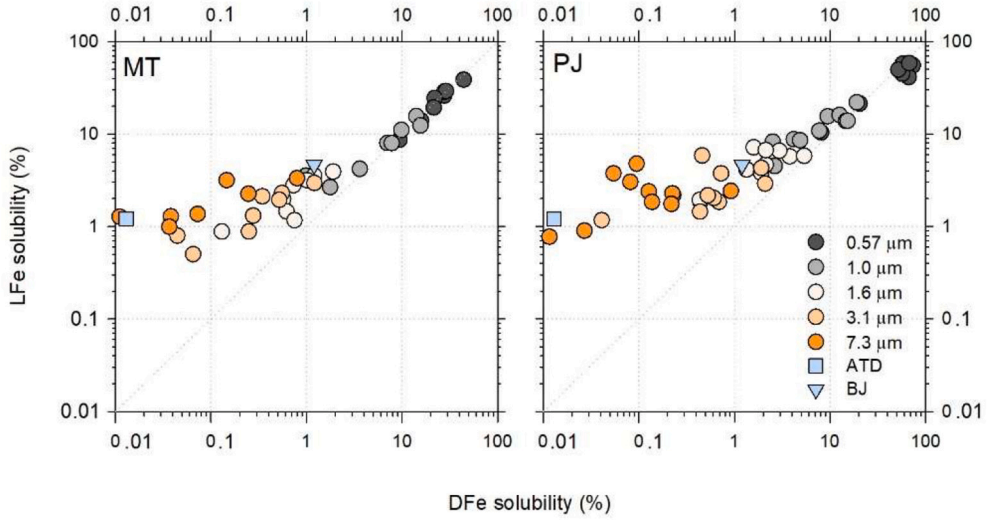

Fig. 5. The comparison of DFe solubility with LFe solubility among size-fractionated aerosols at MT and PJ.

(Table S8).

In brief, fine anthropogenic aerosols would instantly release soluble Fe into seawater but lithogenic particles would need a relatively long time to leach dissolvable Fe to seawater by organic ligand complexion, presented by the buffer leach. The LFe availability would then depend on the capacity of organic ligands available in the water. Thus, the residence time of aerosol particles and the ligand capacity in seawater would be critical factors on deciding their Fe solubility. Perron et al. (2020b) proposed that the 1-h buffer leaching protocol is based on the comparable solubility observation obtained by using strong ligand treatment for 24 h (Clough et al., 2019). Kessler et al. (2020) reported that the solubilities of total suspended particles increased 2-fold from 1 to 8 days by using siderophore desferrioxamine-B (DFOB) as Fe complexation ligand. Based on ^{234}Th and sediment trap data, Black et al. (2020) estimated that the residence time of 75% lithogenic aerosol particles in oceanic surface water range from 10 to 100 days. For future studies, long term laboratory leaching experiments may be required to better estimate the fluxes of LFe.

3.4. The fluxes of DFe and LFe and the overestimate

The deposition velocities of dry aerosols are known to be size dependent and may vary for a couple of orders of magnitude between fine and coarse aerosols (Slinn and Slinn, 1980). Generally, the velocities used range from 0.03 to 0.3 and from 0.3 to 3 cm s^{-1} for fine and coarse aerosols, respectively (Duce et al., 1991). As most of the previous

studies did not carry out size-fractionated aerosol sampling, the dry aerosol Fe deposition fluxes were commonly estimated by multiplying concentrations of total aerosol Fe with an 'averaged' deposition velocity. For example, Buck et al. (2013) used 1.16 cm s^{-1} to calculate total and dissolvable aerosol Fe deposition fluxes in the Pacific Ocean.

Since the larger the sizes are, the higher the deposition velocities would be, the fluxes of coarse aerosols would be weighted more in comparison to concentrations (or masses) among different sizes. The weighting extents for the flux estimate would be dependent on the quantitative information of the masses for size-fractionated aerosols in TFe, LFe, and DFe. In terms of the masses of TFe, coarse aerosols accounted for 68% and 76% at MT and PJ, respectively. In terms of the fluxes, considering the deposition velocities of aerosol sizes, the contribution of coarse aerosols at MT and PJ would up to 97 and 98%, respectively. The averaged TFe fluxes were 3.8, 15, 94, 1286, and 2536 nmol m^{-2} day^{-1} at MT and 1.7, 6.2, 41, 875, and 2547 nmol m^{-2} day^{-1} at PJ for aerosols from size 0.57 to 7.3 μm (Fig. 6, Table S10), respectively. For the fluxes of LFe, the contribution of coarse aerosols becomes dominant, which were 94% and 95% at MT and PJ, respectively, in comparison to 31% and 38% on the masses. The LFe fluxes were 0.82, 0.93, 1.6, 15, and 39 nmol m^{-2} day^{-1} at MT and 0.59, 0.60, 1.6, 18, and 44 nmol m^{-2} day^{-1} at PJ from size 0.57 to 7.3 μm (Fig. 6, Table S10), respectively. For the fluxes of DFe, the contribution of fine aerosols decreased in comparison to the contribution on masses. In comparison to 6.4% of aerosol mass at MT and 10% at PJ, the contribution of coarse aerosols for the fluxes increased to 72% and 77% at MT and PJ, respectively, with averaged fluxes to be 0.85, 0.72, 0.49, 3.2, and 2.1 and 0.66, 0.45, 0.69, 4.5, and 1.4 nmol m^{-2} day^{-1} for MT and PJ from size 0.57 to 7.3 μm, respectively (Fig. 6, Table S10). In brief, the quantitative information of the masses for each aerosol size is essential to obtain an accurate estimate of the fluxes.

Since the relative contribution of each size fraction on the masses of TFe, DFe, and LFe varies dramatically (Fig. 2), the averaged velocities calculated from the individual size in this study vary significantly among the three different fractions, TFe, LFe, and DFe, which were 0.45, 0.22, and 0.045 cm s^{-1} at MT and 0.76, 0.38, and 0.097 cm s^{-1} at PJ, respectively. Without knowing the relative contribution, single deposition velocity, which is commonly used in most of the published field studies, would cause significant bias for the flux estimates. For aerosol samples with a relatively high percentage of fine particles, a general single deposition velocity would tend to overestimate the fluxes of DFe due to their relatively high solubility but relatively low deposition velocity. Table 3 exhibits the fluxes estimated by using individually size-fractionated deposition velocities and the offsets from the fluxes estimated by either using fine and coarse averaged or total averaged velocities. In terms of dissolved fluxes, the value obtained by fine/coarse and total averaged velocities are 1.7- and 9.8-fold of the value obtained by 5 size-fractionated velocities at MT, and are 1.5- and 7.8-fold at PJ, respectively. In terms of labile Fe fluxes, the values were 1.02- and 2.0-fold at MT and 1.07- and 2.0-fold at PJ, respectively. The offset of the fluxes obtained by fine/coarse averaged velocity is significantly smaller than the one estimated by total averaged velocity. With the relatively high percentage of labile Fe in large aerosols, the value of labile Fe estimated by fine/coarse velocities is only 2 to 7% higher than the value estimated by size-fractionated velocity (Table 3). These results show that the information of aerosol size spectrum and their solubilities are essential to obtain reliable dissolvable Fe fluxes, particularly in the oceanic regions where fine anthropogenic aerosols are the dominant fraction.

Table 3
Sensitivity test for the flux calculation of DFe and LFe by using different deposition velocities. The offset (%) is defined as the percentage of the difference (between the fluxes obtained by the two or single velocities and the fluxes obtained by the size-fractionated velocities) to the fluxes obtained by the size-fractionated velocities.

Sampling site	Velocity*	Fe flux (nmol m^{-2} day^{-1})			
		DFe	Offset (%)	LFe	Offset (%)
MT	Size-fractionated	50	0	241	0
	Fine & coarse avg	106	74	284	2
	Total avg	286	880	455	100
PJ	Size-fractionated	45	0	202	0
	Fine & coarse avg	81	46	234	7
	Total avg	220	680	368	102

* Size-fractionated velocities used for flux calculations from size cut-offs 0.57 μm to 7.3 μm were 0.008, 0.018, 0.063, 0.39, 0.94 cm s^{-1} at MT and 0.010, 0.019, 0.070, 0.59, 1.3 cm s^{-1} at PJ, respectively. The fine and coarse average velocities were 0.041 and 0.63 cm s^{-1} at MT and 0.046 and 0.98 cm s^{-1} at PJ, respectively. The total average velocity were 0.45 and 0.76 cm s^{-1} for MT and PJ, respectively.

3.5. Implications to the estimates of global Fe fluxes

Our study demonstrates that sufficient size-fractionated sampling is required to accurately estimate the fluxes of dissolved and labile aerosol Fe. Table 4 compiles the studies with the data of aerosol Fe concentrations and fluxes estimated by using different leaching protocols. Either

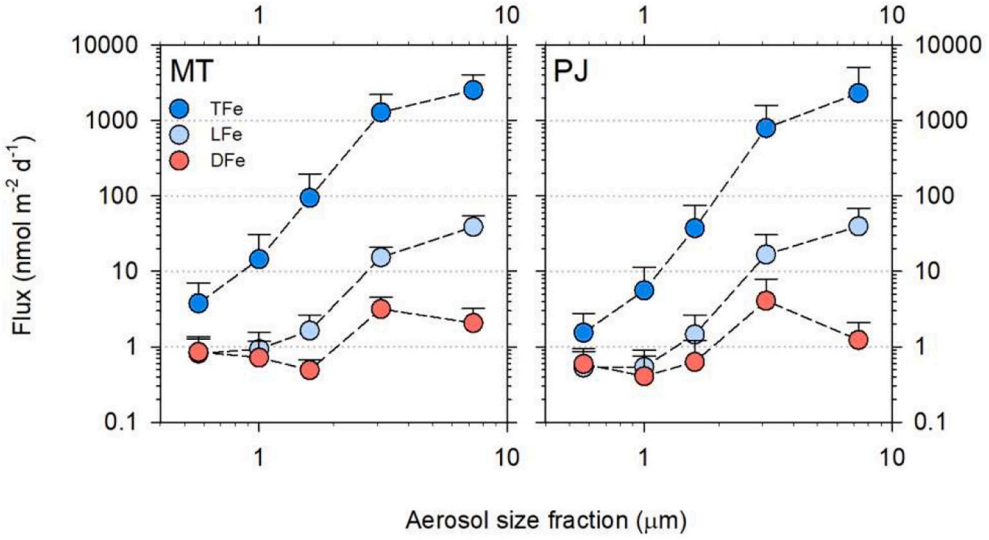

Fig. 6. The comparison of the averaged fluxes of DFe, LFe, and TFe of the size-fractionated aerosols at MT and PJ (Table S10).

Table 4
The comparison of the concentrations and the deposition fluxes of TFe, DFe, LFe, and DFe/TFe in dry aerosols of this study and some of the previous studies.

Sampling site	Size no.	Fe conc. (pmol m^{-3})			DFe/TFe (%)	Fe flux (nmol m^{-2} day^{-1})			DFe/TFe (%)
		TFe	DFe	LFe		TFe	DFe	LFe	
MT, ECS	5	10100	190	300	1.9	3920	7	58	0.19
PJ, ECS	5	5400	130	210	2.4	3150	7	59	0.22
NWPO[a]	2	355	12	n.a.	3.4	265	4	n.a.	1.6
YECS[b]	11	9700	620[#]	n.a.[*]	6.4	8380	466[#]	n.a.	5.6
NWPO[b]	9	2080	110[#]	n.a.[*]	5.3	890	52[#]	n.a.	5.8
NWPO[c]	1	460	44	n.a.	9.6	461	44	n.a.	9.5
NEPO[c]	1	164	13	n.a.	7.9	165	13	n.a.	7.9

a,b,c

[*] n.a.: not available.

[#] The samples were ultrasonically extracted in Milli-Q for 40-min.

[a,b,c] The data are from the studies of Kurisu et al. (2021), Yang et al. (2020), and Buck et al. (2013), respectively. High aerosol events are excluded from the dataset of Buck et al. (2013).

in marginal seas or the open oceans, while only collecting total suspended particles, we found that the ratios of dissolved to total Fe concentrations are comparable to the ratios of their corresponding fluxes, indicating that the two flux estimates were based on onesame average deposition velocity, which was tended to be weighted or biased by coarse fraction. However, once five size-dependent deposition velocities are applied for the estimate, our data indicate that the flux ratios are only one-tenth of the concentration ratios (Table 4). In order to accurately estimate DFe or LFe fluxes, the deposition velocities used have to be size dependent. For studies without size-fractionated information, we suggest using fine aerosol deposition velocity to estimate dissolved Fe fluxes because dissolved Fe mainly originates from fine aerosols, with the exception for samples dominated by lithogenic particles in fine aerosols. For the estimate of LFe fluxes, both the solubilities of DFe and LFe should be determined. Then, two different velocities can be applied to estimate the fluxes: including the dissolved Fe fraction mainly from fine aerosols, [DFe], and the fraction between the labile and dissolved concentrations mainly from coarse aerosols, [LFe] - [DFe].

$$[\mathrm{LFe}] = [\mathrm{DFe}] + ([\mathrm{LFe}] - [\mathrm{DFe}])$$

$$F_{\mathrm{LFe}} = [\mathrm{DFe}] \times V_{d\_Fine} + ([\mathrm{LFe}]\text{–}[\mathrm{DFe}]) \times V_{d\_Coarse}$$

where [LFe] and [DFe] stand for the concentrations of LFe or DFe; F_{LFe} refers to the flux of LFe; V_{d_Fine} and V_{d_Coarse} represent the dry deposition velocities of fine and coarse aerosols.

Only a few studies collected size-fractionated aerosols in large scale cross basin studies. Buck et al. (2010) surveyed DFe in the Northern Atlantic Ocean, and Gao et al. (2019) reported LFe solubility and fluxes in the Arctic Ocean. Both studies reported one kind of solubility only, either DFe or LFe. In addition, DFe stands for instantly dissolved aerosol Fe and LFe solubility is supposed to be closely associated with organic ligand availability in the surface water. While oceanic surface water receiving a large amount of aerosol input, organic ligands may be fully saturated by DFe, such as the pulse events of dust storms (Meskhidze et al., 2017). To fully understand Fe cycling mechanisms among dissolved Fe, abiotic and biotic particulate Fe in the surface ocean would rely on the information of dissolved and labile Fe fluxes of aerosols, organic ligand concentrations, and the residence time of the particles. Thus, it is essential to measure both dissolved and labile Fe solubilities in size-fractionated aerosols in the global ocean.

In brief, the size-dependent distribution patterns of DFe, LFe, or TFe vary dramatically so that the averaged deposition velocities also vary significantly among the three pools in the East China Sea. We found that either single or two averaged deposition velocities that are used in most of previous studies may significantly overestimate dissolvable Fe fluxes in regions with a significant contribution of fine anthropogenic aerosols. The findings of this study show that size-fractionated sampling is critical for the estimate of aerosol dissolvable Fe fluxes for both DFe and LFe. Aerosol sizes are essential and powerful parameters to obtain a more accurate estimate for the solubility and the fluxes of aerosol dissolvable Fe.

Declaration of Competing Interest

None.

Acknowledgments

We thank three anonymous reviewers for their constructive comments, which have significantly improved the quality of this manuscript. We appreciate the technical assistance of K.P. Chiang for aerosol sampling in this study. This study was financially supported by grants MOST 108-2611-M-001-006-MY3 and 108-2923-M-001-009-MY3 from Taiwan Ministry of Science and Technology and by Investigator Award AS-IA-110-M03 from Academia Sinica to T.-Y. Ho.

Appendix A. Supplementary data

Supplementary data to this article can be found online at https://doi.org/10.1016/j.marchem.2022.104106.

References

Baker, A.R., Jickells, T.D., Witt, M., Linge, K.L., 2006. Trends in the solubility of iron, aluminium, manganese and phosphorus in aerosol collected over the Atlantic Ocean. Mar. Chem. 98 (1), 43–58. https://doi.org/10.1016/j.marchem.2005.06.004.

Baker, A.R., et al., 2016. Trace element and isotope deposition across the air-sea interface: progress and research needs. Philos Trans A Math Phys. Eng. Sci. 374 (2081) https://doi.org/10.1098/rsta.2016.0190.

Baker, A.R., Li, M., Chance, R., 2020. Trace metal fractional solubility in size-segregated aerosols from the tropical eastern Atlantic Ocean. Glob. Biogeochem. Cycles 34 (6). https://doi.org/10.1029/2019gb006510.

Baker, A.R., et al., 2021. Changing atmospheric acidity as a modulator of nutrient deposition and ocean biogeochemistry. Sci. Adv. 7 (28) https://doi.org/10.1126/sciadv.abd8800.

Black, E.E., et al., 2020. Ironing out Fe residence time in the dynamic Upper Ocean. Glob. Biogeochem. Cycles 34 (9). https://doi.org/10.1029/2020gb006592.

Buck, C.S., Landing, W.M., Resing, J.A., Lebon, G.T., 2006. Aerosol iron and aluminum solubility in the Northwest Pacific Ocean: results from the 2002 IOC cruise. Geochem. Geophys. Geosyst. 7 (4) https://doi.org/10.1029/2005gc000977.

Buck, C.S., Landing, W.M., Resing, J.A., 2010. Particle size and aerosol iron solubility: a high-resolution analysis of Atlantic aerosols. Mar. Chem. 120 (1–4), 14–24. https://doi.org/10.1016/j.marchem.2008.11.002.

Buck, C.S., Landing, W.M., Resing, J., 2013. Pacific Ocean aerosols: deposition and solubility of iron, aluminum, and other trace elements. Mar. Chem. 157, 117–130. https://doi.org/10.1016/j.marchem.2013.09.005.

Chou, C.C.K., et al., 2008. Implications of the chemical transformation of Asian outflow aerosols for the long-range transport of inorganic nitrogen species. Atmos. Environ. 42 (32), 7508–7519. https://doi.org/10.1016/j.atmosenv.2008.05.049.

Clough, R., Lohan, M.C., Ussher, S.J., Nimmo, M., Worsfold, P.J., 2019. Uncertainty associated with the leaching of aerosol filters for the determination of metals in aerosol particulate matter using collision/reaction cell ICP-MS detection. Talanta 199, 425–430. https://doi.org/10.1016/j.talanta.2019.02.067.

Cutter, G., et al., 2017. Sampling and sample-handling protocols for GEOTRACES. Cruises 3. https://doi.org/10.25607/OBP-2.

Duce, R.A., et al., 1991. The atmospheric input of trace species to the world ocean. Glob. Biogeochem. Cycles 5 (3), 193–259. https://doi.org/10.1029/91gb01778.
Emerson, E.W., et al., 2020. Revisiting particle dry deposition and its role in radiative effect estimates. Proc. Natl. Acad. Sci. U. S. A. 117 (42), 26076–26082. https://doi.org/10.1073/pnas.2014761117.
Foret, G., Bergametti, G., Dulac, F., Menut, L., 2006. An optimized particle size bin scheme for modeling mineral dust aerosol. J. Geophys. Res. 111 (D17) https://doi.org/10.1029/2005jd006797.
Gao, Y., et al., 2019. Particle-size variability of aerosol Iron and impact on Iron solubility and dry deposition fluxes to the Arctic Ocean. Sci. Rep. 9 (1), 16653. https://doi.org/10.1038/s41598-019-52468-z.
Gao, Y., et al., 2020. Particle-size distributions and solubility of aerosol Iron over the Antarctic peninsula during austral summer. Journal of Geophysical Research: Atmospheres 125 (11). https://doi.org/10.1029/2019jd032082.
Ho, T.Y., Chien, C.T., Wang, B.N., Siriraks, A., 2010. Determination of trace metals in seawater by an automated flow injection ion chromatograph pretreatment system with ICPMS. Talanta 82 (4), 1478–1484. https://doi.org/10.1016/j.talanta.2010.07.022.
Hsu, S.-C., et al., 2010. Sources, solubility, and dry deposition of aerosol trace elements over the East China Sea. Mar. Chem. 120 (1–4), 116–127. https://doi.org/10.1016/j.marchem.2008.10.003.
Hu, Z.C., Gao, S., 2008. Upper crustal abundances of trace elements: a revision and update. Chem. Geol. 253 (3–4), 205–221. https://doi.org/10.1016/j.chemgeo.2008.05.010.
Jickells, T.D., et al., 2005. Global iron connections between desert dust, ocean biogeochemistry, and climate. Science 308 (5718), 67–71. https://doi.org/10.1126/science.1105959.
Jickells, T.D., Baker, A.R., Chance, R., 2016. Atmospheric transport of trace elements and nutrients to the oceans. Philos Trans A Math Phys Eng. Sci. 374 (2081) https://doi.org/10.1098/rsta.2015.0286.
Kessler, N., Kraemer, S.M., Shaked, Y., Schenkeveld, W.D.C., 2020. Investigation of Siderophore-promoted and reductive dissolution of dust in marine microenvironments such as Trichodesmium colonies. Front. Mar. Sci. 7 https://doi.org/10.3389/fmars.2020.00045.
Kurisu, M., Takahashi, Y., Iizuka, T., Uematsu, M., 2016. Very low isotope ratio of iron in fine aerosols related to its contribution to the surface ocean. Journal of Geophysical Research: Atmospheres 121 (18), 11,119–11,136. https://doi.org/10.1002/2016jd024957.
Lam, P.J., Ohnemus, D.C., Auro, M.E., 2015. Size-fractionated major particle composition and concentrations from the US GEOTRACES North Atlantic zonal transect. Deep-Sea Res. II Top. Stud. Oceanogr. 116, 303–320. https://doi.org/10.1016/j.dsr2.2014.11.020.
Martin, J.H., 1990. Glacial-interglacial CO2change: the Iron hypothesis. Paleoceanography 5 (1), 1–13. https://doi.org/10.1029/PA005i001p00001.
Martin, J.H., Fitzwater, S.E., 1988. Iron deficiency limits phytoplankton growth in the north-East Pacific subarctic. Nature 331 (6154), 341–343. https://doi.org/10.1038/331341a0.
Matsui, H., et al., 2018. Anthropogenic combustion iron as a complex climate forcer. Nat. Commun. 9 (1), 1593. https://doi.org/10.1038/s41467-018-03997-0.
Mead, C., Herckes, P., Majestic, B.J., Anbar, A.D., 2013. Source apportionment of aerosol iron in the marine environment using iron isotope analysis. Geophys. Res. Lett. 40 (21), 5722–5727. https://doi.org/10.1002/2013gl057713.
Meskhidze, N., Chameides, W.L., Nenes, A., Chen, G., 2003. Iron mobilization in mineral dust: can anthropogenic SO2 emissions affect ocean productivity? Geophys. Res. Lett. 30 (21) https://doi.org/10.1029/2003gl018035.
Meskhidze, N., Hurley, D., Royalty, T.M., Johnson, M.S., 2017. Potential effect of atmospheric dissolved organic carbon on the iron solubility in seawater. Mar. Chem. 194, 124–132. https://doi.org/10.1016/j.marchem.2017.05.011.
Meskhidze, N., et al., 2019. Perspective on identifying and characterizing the processes controlling iron speciation and residence time at the atmosphere-ocean interface. Mar. Chem. 217 https://doi.org/10.1016/j.marchem.2019.103704.
Ohnemus, D.C., et al., 2014. Laboratory intercomparison of marine particulate digestions including piranha: a novel chemical method for dissolution of polyethersulfone filters. Limnology and Oceanography-Methods 12 (8), 530–547. https://doi.org/10.4319/lom.2014.12.530.
Perron, M.M.G., et al., 2020a. Origin, transport and deposition of aerosol iron to Australian coastal waters. Atmos. Environ. 228 https://doi.org/10.1016/j.atmosenv.2020.117432.
Perron, M.M.G., et al., 2020b. Assessment of leaching protocols to determine the solubility of trace metals in aerosols. Talanta 208, 120377. https://doi.org/10.1016/j.talanta.2019.120377.
Quinn, T.L., Ondov, J.M., 1998. Influence of temporal changes in relative humidity on dry deposition velocities and fluxes of aerosol particles bearing trace elements. Atmos. Environ. 32 (20), 3467–3479. https://doi.org/10.1016/s1352-2310(98)00047-8.
Raiswell, R., Canfield, D.E., 2012. The Iron biogeochemical cycle past and present. Geochemical Perspectives 1 (1), 1–220. https://doi.org/10.7185/geochempersp.1.1.
Sakata, K., et al., 2018. Custom-made PTFE filters for ultra-clean size-fractionated aerosol sampling for trace metals. Mar. Chem. 206, 100–108. https://doi.org/10.1016/j.marchem.2018.09.009.
Sarthou, G., et al., 2003. Atmospheric iron deposition and sea-surface dissolved iron concentrations in the eastern Atlantic Ocean. Deep-Sea Res. I Oceanogr. Res. Pap. 50 (10−11), 1339–1352. https://doi.org/10.1016/s0967-0637(03)00126-2.
Schroth, A.W., Crusius, J., Sholkovitz, E.R., Bostick, B.C., 2009. Iron solubility driven by speciation in dust sources to the ocean. Nat. Geosci. 2 (5), 337–340. https://doi.org/10.1038/ngeo501.
Shelley, R.U., Morton, P.L., Landing, W.M., 2015. Elemental ratios and enrichment factors in aerosols from the US-GEOTRACES North Atlantic transects. Deep-Sea Res. II Top. Stud. Oceanogr. 116, 262–272. https://doi.org/10.1016/j.dsr2.2014.12.005.
Shelley, R.U., et al., 2017. Quantification of trace element atmospheric deposition fluxes to the Atlantic Ocean (>40°N; GEOVIDE, GEOTRACES GA01) during spring 2014. Deep-Sea Res. I Oceanogr. Res. Pap. 119, 34–49. https://doi.org/10.1016/j.dsr.2016.11.010.
Sholkovitz, E.R., Sedwick, P.N., Church, T.M., 2009. Influence of anthropogenic combustion emissions on the deposition of soluble aerosol iron to the ocean: empirical estimates for island sites in the North Atlantic. Geochim. Cosmochim. Acta 73 (14), 3981–4003. https://doi.org/10.1016/j.gca.2009.04.029.
Slinn, S.A., Slinn, W.G.N., 1980. Predictions for particle deposition on natural waters. Atmospheric Environment (1967) 14 (9), 1013–1016. https://doi.org/10.1016/0004-6981(80)90032-3.
Tagliabue, A., et al., 2017. The integral role of iron in ocean biogeochemistry. Nature 543 (7643), 51–59. https://doi.org/10.1038/nature21058.
Wang, B.S., Lee, C.P., Ho, T.Y., 2014. Trace metal determination in natural waters by automated solid phase extraction system and ICP-MS: the influence of low level mg and ca. Talanta 128, 337–344. https://doi.org/10.1016/j.talanta.2014.04.077.
Yang, T., et al., 2020. Solubilities and deposition fluxes of atmospheric Fe and cu over the Northwest Pacific and its marginal seas. Atmos. Environ. 239 https://doi.org/10.1016/j.atmosenv.2020.117763.
Zhu, X., Prospero, J.M., Millero, F.J., Savoie, D.L., Brass, G.W., 1992. The solubility of ferric ion in marine mineral aerosol solutions at ambient relative humidities. Mar. Chem. 38 (1–2), 91–107. https://doi.org/10.1016/0304-4203(92)90069-m.